Correlation of H–mode Barrier Width and Neutral Penetration Length

R.J. Groebner,[1] M.A. Mahdavi,[1] A.W. Leonard,[1] T.H. Osborne,[1] N.S. Wolf,[2] G.D. Porter,[2] P.C. Stangeby,[3] N.H. Brooks,[1] R.J. Colchin,[4] W.W. Heidbrink,[5] T.C. Luce,[1] G.R. McKee,[6] L.W. Owen,[4] G. Wang,[7] D.G. Whyte[8*]

[1]General Atomics, P.O. Box 85608, San Diego, California 92186-5608
email: groebner@fusion.gat.com
[2]Lawrence Livermore National Laboratory, Livermore, California 94551
[3]University of Toronto, Toronto, Canada
[4]Oak Ridge National Laboratory, Oak Ridge, Tennessee 37831
[5]University of California, Irvine, California 92697-4574
[6]University of Wisconsin, Madison, Madison, Wisconsin 53706
[7]University of California, Los Angeles, California 90095-1597
[8]University of California, San Diego, 9500 Gilman Drive, La Jolla, California 92093-0417
*Present Address: University of Wisconsin-Madison, Madison, Wisconsin 53706

Abstract. Pedestal studies in DIII–D find a good correlation between the width of the H–mode density barrier and the neutral penetration length. These results are obtained by comparing experimental density profiles to the predictions of an analytic model for the profile, obtained from the particle continuity equations for electrons and deuterium atoms. In its range of validity (edge temperature between 40–500 eV), the analytic model quantitatively predicts the observed decrease of the width as the pedestal density increases, the observed strong increase of the gradient of the density as the pedestal density increases and the observation that L–mode and H–mode profiles with the same pedestal density have very similar shapes. The width of the density barrier, measured from the edge of the electron temperature barrier, is the lower limit for the observed width of the temperature barrier. These results support the hypothesis that particle fueling provides the dominant control for the size of the H–mode transport barrier.

1. Introduction

Experimental observations and theoretical modeling show that the H–mode pedestal has a large impact on tokamak performance [1-3]. Therefore, uncertainties in the scaling of the pedestal lead to significant uncertainties in the performance of next-step machines. For these reasons, understanding the physics of the H–mode pedestal has been an important topic of fusion research for the last several years, and one of the key questions in pedestal research is: What physics sets the width of the H–mode temperature and density barriers?

Self-consistent transport models have been developed which predict that transport barriers are formed by sufficiently large sources of heat, particles or momentum [4,5]. The Hinton-Staebler model [4] predicts that the H-mode transport barrier is primarily driven by the edge particle source. In the model, this source produces a large density gradient which produces a large pressure gradient with an associated radial electric field, which stabilizes turbulence via the E×B mechanism. The width of the transport barrier is predicted to be approximately the neutral penetration depth.

This paper presents results of studies in the DIII–D tokamak to address two basic questions posed by the Hinton-Staebler model. First, is the steep gradient region of the edge density profile produced by the fueling neutrals? A number of studies in DIII–D strongly indicate that the answer is “yes”. These studies are based primarily on the use of an analytic model (Section 2) to study various features of the edge density profile. With standard assumptions about the model parameters, the model is quantitatively consistent with the measured widths (Section 3.2) and gradients (Section 3.3) of the edge density profile over a wide range of densities. Moreover, it is found that L–mode and H–mode density profiles with similar values of the pedestal density have quite similar shapes (Section 3.4). Benchmarking studies (Section 3.5) show that the simple analytic model compares favorably with a much more sophisticated edge modeling code in the regime where charge exchange neutrals are expected to dominate edge fueling. These studies lead to the conclusion that the width of the steep gradient region in the edge density profile is the fueling depth of the neutrals and that this depth is set self-consistently by atomic physics as well as plasma physics.

A second question studied here is: is the width of the H–mode transport barrier approximately equal to the width of the steep gradient region of the density profile? This question is studied by examining the width of the barrier in the electron temperature as compared to the width of the density barrier, with both widths being measured from the foot of the electron temperature barrier. It is found that this ratio is close to but on average slightly greater than one (Section 4). These results are consistent with the density gradient, and therefore the fueling source, providing a lower limit for the transport barrier width. Thus, the experimental findings here are consistent with the basic assertions of the Hinton-Staebler model.

2. Analytical Model for Density Profile

An analytical model has been developed to study the interplay of atomic physics and plasma physics in forming the edge electron density profile. The formulation used here is based on the work of Wagner, Lackner, and Engelhardt [6,7] and the derivation is discussed in detail elsewhere [8–12]. In brief, an equation for the edge electron density profile in slab geometry is obtained from a self-consistent solution of the particle continuity equations for the electrons and the deuterium atoms, with impurities ignored. The flux of electrons Γ_e is assumed to have the form $\Gamma_e = Ddn_e/dx$, where D is the particle diffusion coefficient and x is a spatial coordinate perpendicular to the magnetic surface. The flux of deuterium atoms Γ_n is assumed to have the form $\Gamma_n = n_n V_n$, where n_n is the neutral density and V_n is the inward neutral velocity perpendicular to the magnetic surface. The diffusion coefficient and neutral velocity are assumed to be constant in space. The Wagner-Lackner-Engelhardt model has been extended by allowing for different diffusion coefficients on the open and closed field lines and for a neutral source that is localized in the poloidal direction. Inside the separatrix, the resulting profile for n_e is

$$n_e(x) = n_{e,ped} \tanh\left[C - \left(\sigma_i V_e / 2V_n\right) n_{ped} E\, x\right] \quad , \tag{1}$$

with $n_{e,ped}$ being the pedestal density as $x \rightarrow -\infty$, σ_i being the ionization cross section, V_e being the electron thermal velocity and E being the ratio of the distances between two flux surfaces at the poloidal angle of the particle source and at the poloidal angle θ_m where the measurement is made. The geometric parameter E is in some sense a measure of the efficiency of fueling at a given poloidal location. For typical diverted discharges in DIII–D, the value of E for fueling in the vicinity of the X–point is about an order of magnitude larger than for fueling at the outside midplane. Thus, fueling in the X–point is not favorable for producing large widths in the density profile. Ionization in the scrape-off layer (SOL) is neglected. All ionization occurs inside the LCFS with particles diffusing onto the open field lines, where they are rapidly transported by parallel flow to the divertor and lost. Thus, the SOL physics acts as a sink of particles and helps to set up the gradient of the density profile at and inside the LCFS. This SOL physics is modeled by assuming that n_e has the source-free Yokomizo solution [13]

$$n_e(x) = n_{e,sep} \exp\left(-x / \sqrt{D_s \tau_{\|}}\right) \quad , \tag{2}$$

where $n_{e,sep}$ is the electron density at the separatrix (LCFS), D_s is the diffusion coefficient in the SOL and $\tau_{\|}$ is the average particle lifetime for parallel flow to the divertor plates. The integration constant C in Eq. (1), obtained by continuity of n_e and its first derivative at x=0, is

$$C = 0.5 \sinh^{-1}(U), \quad U = \left[\sqrt{D_s \tau_{\|}}\, \sigma_i V_e / V_n\right] E n_{e,ped}\, D_c / D_s \quad , \tag{3}$$

where D_c is the diffusion coefficient in the core. Equation (1) can be written as

$$n_e(x) = n_{e,ped} \tanh\left[C - x/\Delta_{ne}\right] \quad , \tag{4}$$

with

$$\Delta_{ne} = 2V_n \Big/ \left(\sigma_i V_e E n_{e,ped}\right) \quad . \tag{5}$$

It is straightforward to show [9] that Δ_{ne} is also the characteristic attenuation length for the neutrals, as measured from the LCFS. Thus, the model predicts that the scale lengths for the rise of the electron density and the penetration of the neutrals are essentially the same. The separatrix density has a finite value as given by

$$n_{e,sep} = n_{e,ped}\tanh[C] \quad , \tag{6}$$

One of the major limitations of this model is that the possibility for neutral diffusion due to multiple charge exchange events is ignored due to the intractability of this physics in an analytic model. The omission of this physics restricts the applicability of the model to edge temperatures in the approximate range 40–500 eV, in which the ionization rate is comparable to the charge exchange rate.

3. Comparison of Data to Analytical Model

The analytic model discussed in the previous section can be used to make predictions, useful for comparison with data, and these will be discussed here.

3.1. Evaluating the Analytical Model

For a given value of $n_{e,ped}$, the model predicts that the density inboard of the LCFS depends on five free parameters: D_C, D_S, E, V_n, and T_e (used to compute σ_i and V_e). Nominal values of these parameters are chosen as follows. Based on typical results of edge modeling analysis, nominal values of D_C and D_S are taken as 0.14 and 0.4 m^2/s, respectively. As will be shown later, the widths and gradients have a very weak dependence on the diffusion coefficients, and the results are quite insensitive to the choice of these parameters. The nominal value of T_e is taken as 75 eV, a representative value at the LCFS. The geometric factor E will ultimately be chosen to give best consistency with the data, as discussed later. However, modeling of the pedestal and SOL density profile, as performed with the edge modeling code UEDGE [14] suggests that a typical value of E is in the range of 6–8 with fueling occurring in the vicinity of the X–point and measurements being made at the outboard midplane. Specification of the neutral velocity V_n is based on the assumption that neutrals arriving at the LCFS have two distributions: those which are Frank-Condon neutrals with temperatures of ~ 3 eV and those which have charge-exchanged with plasma ions and have approximately the ion temperature, in rough accord with typical experimental observations. At sufficiently low plasma densities, neutrals at the LCFS will be predominantly Frank-Condon neutrals and at sufficiently high densities they will be predominantly charge-exchange neutrals. A simple fluid model has been developed to compute the ratio of the density of charge-exchange neutrals to Frank-Condon neutrals and the V_n is computed as the average inward velocity of the resulting neutral populations [12].

3.2. Scaling of Width of Density Profile

Equation (5) shows that the width parameter Δ_{ne} depends on both atomic physics and plasma physics parameters. However, for fixed temperatures and fixed fueling location, Eq. (5) predicts that $\Delta_{ne} \sim 1/n_{e,ped}$. Experimental data can be used to test this prediction. Moreover, with an appropriate estimate for the geometric factor E, a quantitative comparison can be made between theory and experiment. Widths of experimental density profiles W_{ex} are obtained by fitting functions with a hyperbolic tangent shape (plus appropriate linear terms) [15] to electron density profiles obtained with the DIII–D multi-pulse Thomson scattering system [16]. A complication in comparing these widths with the model is that W_{ex} includes not only that part of the width of the density barrier that lies inside the LCFS but also that part of the width that lies outside the LCFS. In contrast, the width parameter Δ_{ne} in the model lies entirely inside the LCFS. Thus, W_{ex} is not necessarily a good approximation of Δ_{ne}. In principle, it is desirable to compute an experimental value for Δ_{ne} by subtracting that part of the width which lies outside the LCFS from the experimental meausurement of W_{ex}. In practice, this approach requires the determination of the location of the LCFS from an equilibrium construction. This determination has potential errors of up to 1 cm, which are

comparable to the widths being measured. Thus, computing an experimental value for Δ_{ne} tends to add scatter to the data and somewhat obscure trends which are more obvious when the entire experimental width W_{ex} is plotted. Because of this difficulty, a theoretical width W_{th} has been defined to emulate the experimental width W_{ex}. W_{th} is defined as the distance over which the model density profile, with a tanh form, varies from 88% of $n_{e,ped}$ to 12% of $n_{e,ped}$.

Theoretical widths W_{th} computed from the model compare well with W_{ex} from experimental data, as shown in Fig. 1. The data are obtained from systematic scans of $n_{e,ped}$ in which large plasma-wall gaps were maintained to ensure that fueling always occurred from the same poloidal location, gas fueling was used to increase the density and cryopumping was used to reduce the density. The data are averaged over 50-300 ms in order to reduce scatter, presumably due to turbulence, and data with ELMs are eliminated. Edge temperatures were in the range of applicability of the model. For the evaluation of W_{th}, the free parameters were given the values as discussed in 3.1. Evaluation of W_{th} generally requires computation of the density profile in the SOL with the aid of Eq. (2). For this purpose, the average particle lifetime in the SOL $\tau_{||}$ is given a value representative of typical discharges used in the study. Results are quite insensitive to the exact value of $\tau_{||}$. The geometric parameter E was chosen as 7 to give a "best" fit of the model to the data.

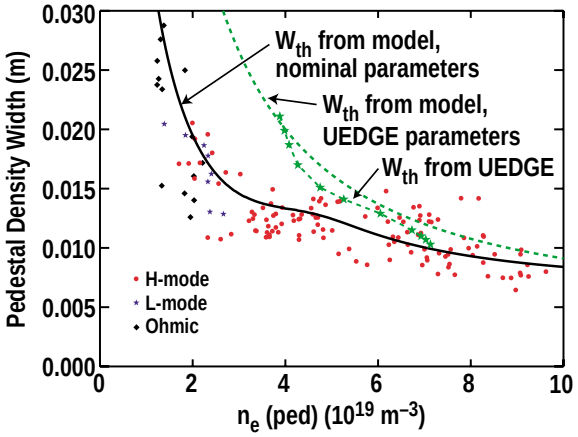

Fig. 1. Widths of edge density profile, normalized to outboard midplane, vs pedestal density. Experimental widths from H–mode (red circles), L–mode (blue stars) and Ohmic (black diamonds) discharges. Solid black curve is theoretical width W_{th} with parameters at nominal values with Frank-Condon neutrals included. Green stars and dashed curve are widths from UEDGE modeling. Dashed green curve is width from analytic model, using UEDGE parameters, with Frank-Condon neutrals ignored.

The experimental widths show a systematic decrease as the pedestal density increases, a qualitative behavior expected from Eq. (5). One feature of the data is that there is a flattening of this trend for $n_{e,ped}$ in the range $2–4\times10^{19}$ m^{-3}. This flattening is understood as a transition between a low density regime, in which the fueling is dominated by Frank-Condon neutrals, and a high density regime, in which charge exchange neutrals dominate the fueling. Figure 1 includes data from Ohmic, L–mode and H–mode discharges. For the range of $n_{e,ped}$ in which L–mode and H–mode data are simultaneously obtained, about $2–3\times10^{19}$ m^{-3}, the widths are virtually the same, despite the fact that the edge transport is markedly different for the two regimes. These data provide strong evidence that the width of the H–mode density barrier cannot be understood purely in terms of the diffusion coefficient. The model used here, which includes self-consistently the particle source, is consistent with these results.

3.3. Scaling of Gradient of Density Profile

The analytic model can also be used to compute the maximum gradient of the edge density profile and the results compare favorably with the data. From Eq. (4), it can be shown that the gradient inboard of the LCFS is

$$\partial n_e(x)\big/\partial x = -\left(n_{e,ped}/\Delta_{ne}\right)\mathrm{sech}^2\left[C - x/\Delta_{ne}\right] \quad . \tag{7}$$

The argument of the sech is always positive inside the LCFS; therefore, the gradient reaches its maximum value at the LCFS. For small C, obtained when the separatrix density is small relative to the pedestal density, the maximum gradient is approximately $\max(-\nabla n_e)_{th}=n_{e,ped}/\Delta_{ne}$. In contrast to the widths, which show relatively little variation with $n_{e,ped}$ for H–mode data, the gradient is predicted to vary strongly, approximately as $n_{e,ped}^2$.

The maximum gradient from the experiment $\max(-\nabla n_e)_{ex}$ is easily calculated from fits to the data. A comparison of the data and the model prediction is shown in Fig. 2, which uses the same experimental data set and the same model parameters as used in Fig. 1. The gradients are mapped to the outboard midplane. The model, which includes Frank-Condon neutrals, shows very good agreement with the data.

As in the case of the widths, the experimental gradients for L–mode and H–mode data overlap in the region of overlapping $n_{e,ped}$, despite the fact that transport is very different for the H–mode and L–mode data. The analytic model, which passes nicely through the data, shows how this is possible. The gradient at the LCFS depends on the diffusion coefficients only through the parameter C in Eq. (7). Since transport does not enter directly into the width parameter, it can only affect the gradient (at fixed $n_{e,ped}$) by increasing C and therefore the value of the density at the LCFS. The resulting change in the gradient is quite moderate.

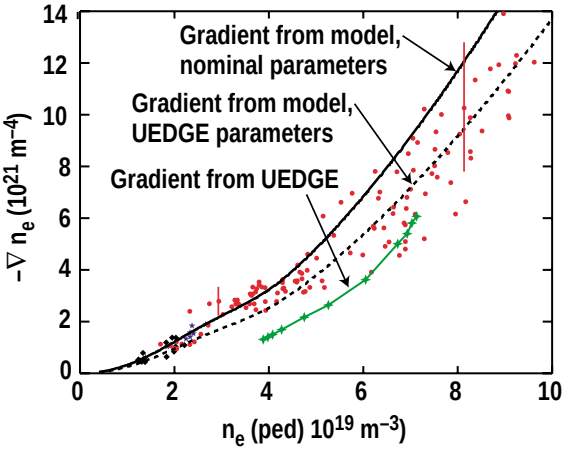

Fig. 2. Maximum gradients of edge density profile, normalized to outboard midplane, versus pedestal density. Experimental gradients from H–mode (red circles), L–mode (blue stars) and Ohmic (black diamonds) discharges. Solid black curve is model gradient with nominal parameters. Green stars are gradients from UEDGE modeling and dashed curve is model gradient, using UEDGE parameters. Vertical red bars represent range of scatter of averaged data.

3.4. Comparison of L–mode and H–mode Profiles

Another way of illustrating the prediction of Eq. (5), that for fixed $n_{e,ped}$ the width inboard of the LCFS is independent of diffusion, is to compare density profiles of L–mode and H–mode discharges with the same $n_{e,ped}$. As illustrated in Fig. 3, L–mode and H–mode profiles with the same $n_{e,ped}$ have been obtained with the aid of cryopumping to reduce the density in the H–mode discharge and gas-puffing to increase the density in the L–mode discharge. In these profiles, the width parameters, as measured from the LCFS to the inner part of the density barrier where profile flattening starts to occur, are very similar, as predicted by Eq. (5). The major difference between the two profiles is that the separatrix density for the L–mode profile is significantly higher than for the H–mode discharge. This feature is consistent with the model and can be understood as a result of higher transport in the L–mode, as discussed in 3.3. This effect has been successfully modeled, as shown in Fig. 3(b), by producing two model profiles with identical parameters except that D_c and D_s were increased by an order of magnitude for one of the profiles. These model profiles show the same features as seen in the experimental data: the widths inside the LCFS are nearly identical and the separatrix density is higher for the profile with higher transport. Although these profiles are similar, there is an important difference in the dynamics. The particle flux (neutral density) was an order of magnitude higher for the profile with high diffusion coefficient than for the profile with low diffusion coefficient.

3.5. Benchmarking of Analytic Model

One potential objection to the analytic model is that it over-simplifies the complex fueling process to such a degree that the model is of little use. This objection has been addressed with benchmarking of results of the analytic model to results from the sophisticated edge-modeling code UEDGE [14], and the comparison shows that the analytic model is in reasonable agreement with UEDGE [17]. The UEDGE code is a 2-D fluid code that solves the plasma transport equations at the very edge of the core plasma and on the open field lines in the actual geometry of the non-circular DIII–D plasmas. UEDGE contains a fluid neutrals model which follows neutrals from their release at the divertor plates and walls of the vacuum

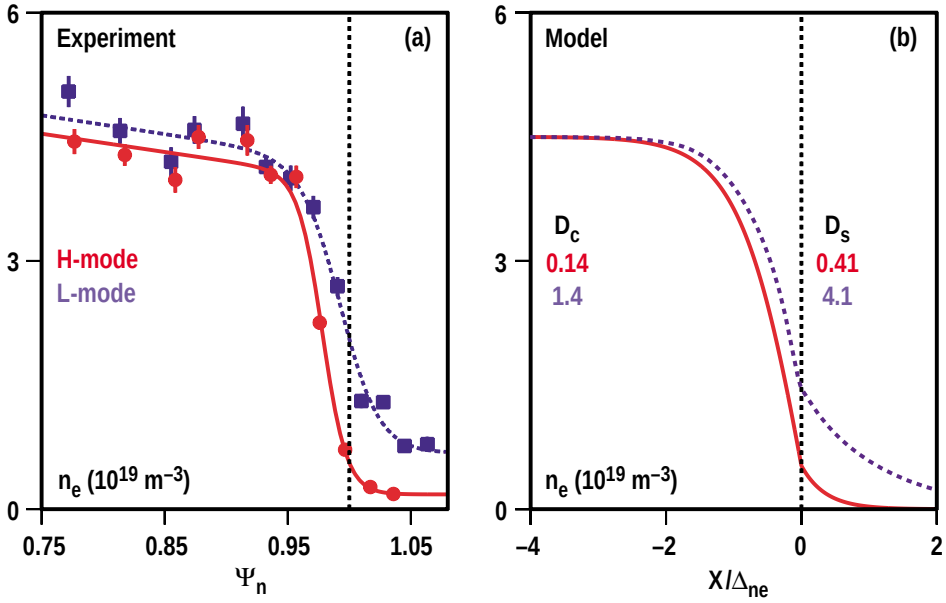

Fig. 3. Comparison of edge density profiles with same pedestal density. (a) Experimental L–mode (squares plus dashed line) and H–mode (circles plus solid line) profiles shown as functions of poloidal flux. (b) Density profiles computed from model and plotted versus normalized physical distance. Model parameters for dashed curve are same as for solid curve except that D_S and D_C are increased by 10×.

vessel to the point of absorption in the plasma. Only charge-exchange neutrals are included in the present version of the model. The plasma transport is modeled by specifying the transport coefficients.

Figures 1 and 2 show that the widths and maximum gradients, as obtained from the analytic model and from the UEDGE simulations, are in reasonable agreement. In the comparisons that were performed, the pedestal density was varied in the UEDGE code over the range $4–7.5\times10^{19}$ m^{-3} with the core and SOL diffusivities set to 0.075 m^2/s [17]. Heating power was held constant, resulting in the separatrix T_i varying in the range 0.15–0.6 keV. The curves from the analytic model were computed with the same diffusion coefficient, with the separatrix T_i fixed to 0.15 keV and the flux expansion factor fixed at 5.5, with the range from the UEDGE runs being 5–6. Quantitative tests can be performed by obtaining the maximum gradient of the UEDGE profiles and by fitting the tanhfit function to these profiles to obtain width parameters. For $n_{eped} \geq 4.5\times10^{19}$ m^{-3}, the widths from the two calculations agree within 10-20% and the maximum gradients agree within ~ 20%–50%. The larger differences between the two models for the gradients than for the widths indicates that the physics differences between the models show up as the profiles are examined in higher order detail. The comparison of the gradients is quite good, given that the gradients vary by over a magnitude in the experiment. The agreement between UEDGE and the data starts to diverge somewhat for $n_{eped} \leq 4.5\times10^{19}$ m^{-3}. This is understood as due to the importance of Frank-Condon neutrals, ignored by UEDGE, for these lower densities. In summary, the comparison between the two models is good in the range where good agreement is expected and these results support the use of the analytic model for studying the systematics of the edge electron density profile.

4. Comparison of Transport Barrier Width and Density Width

The previous discussion strongly indicates that the width of the density “barrier”, the region of steep gradient in the density, is primarily a measure of the fueling depth. Thus, it cannot necessarily be concluded that the width of the density barrier is a measure of the width of the transport barrier. On the other hand, the Hinton-Staebler model predicts that the width of the transport barrier should be comparable to the fueling depth. Experimental data are used here to test this prediction, and the analysis is consistent with this prediction.

The width of the electron temperature barrier, as measured with fits of the tanh function, is used as a measure of the width of the transport barrier. The outer edge of the temperature barrier is generally taken as a good measure of the location of the LCFS and thus this width will be called Δ_{Te}. For this comparison, it is necessary to have an estimate of the density width Δ_{ne} that is inside the LCFS. This estimate is obtained by measuring the distance between the outer edge of the electron temperature barrier to the inner edge of the density barrier. The ratio of widths Δ_{Te}/Δ_{ne} can be computed and the result is shown in the histogram of Fig. 4. The data for Fig. 4 are the H–mode data used in Figs. 1 and 2; averaging has not been performed in Fig. 4, so many more data points are available than for Figs. 1 and 2. For each bin of the quantity Δ_{Te}/Δ_{ne}, the histogram shows the number of times the ratio was found to be in that bin. The histogram shows clearly that Δ_{Te} is almost always between 1 and 2 times Δ_{ne} with the most probable value being about 1.1–1.2 times Δ_{ne}. There are very few data points with a ratio below one and these are within experimental error of being one. Thus, the data show that extent of the density barrier inside the LCFS forms a lower bound for the extent of the transport barrier; the transport barrier can extend up to another Δ_{ne} into the plasma.

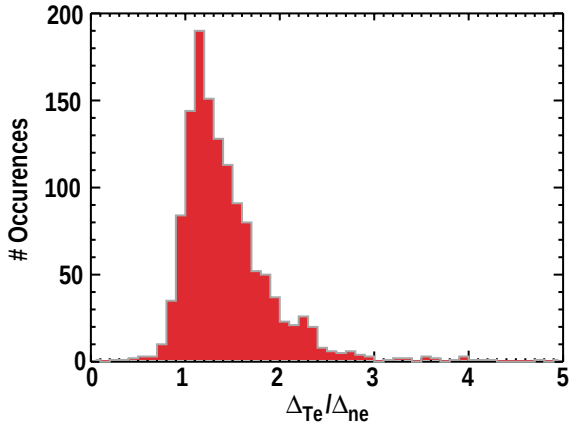

Fig. 4. Histogram showing number of occurrences of various ratios of electron temperature barrier width to electron density barrier width. Outer edge of density barrier is taken as outer edge of temperature barrier.

5. Conclusions and Discussion

The data and analysis presented here strongly indicate that the width of the steep gradient region in the edge H–mode density profile is approximately equal to the fueling depth, which is set self-consistently by the edge particle transport and neutral transport. With the fueling adjusted to produce a given pedestal density, the resulting width and maximum gradient of the density profile are weakly dependent on the magnitude of the transport, with the effect of transport showing up most prominently at the separatrix. These conclusions are based on the comparison of experimental widths and gradients of the density profile with predictions of an analytic model based on a self-consistent solution of the particle and neutral transport. These conclusions also follow from the fact that L–mode density profiles also have substantial gradients at the plasma edge, even though no transport barrier is known to exist. L–mode and H–mode profiles with the same pedestal density have very similar widths and gradients, as expected from the self-consistent model.

The H–mode profiles in DIII–D are also consistent with the prediction of the Hinton-Staebler model that the width of the transport barrier is controlled primarily by the particle source. The evidence is that the most probable width of the electron temperature barrier is very nearly equal to the width of the density barrier inside the last closed flux surface. However, the transport barrier can extend up to two times the width of the density barrier, indicating that fueling provides a lower bound on the size of the transport barrier. In the context of the Hinton-Staebler model, the heat flux from the core may also be providing some control of the transport barrier.

An important implication of the theoretical model and results presented here is that techniques to modify the fueling might provide means to control the width of the transport barrier. In particular, a technique which provides deeper fueling than conventional gas-puffing might produce a density barrier which is wider than conventional H–mode barriers.

Acknowledgments

The authors gratefully acknowledge the assistance of the entire DIII–D staff in obtaining these results and express their appreciation to T. Taylor and R. Stambaugh in supporting this work. Work supported by U.S. Department of Energy under Contracts DE-AC03-99ER54463, W-7405-ENG-48, DE-0AC05-96OR22464, SC-G903402, and Grants DE-FG03-01ER54615 and DE-FG03-95ER54294.

References

[1] OSBORNE, T.H., *et al*., Proc. 24th Eur. Conf on Controlled Fusion and Plasma Physics, Berchtesgaden, Germany, 1997 (European Physical Society, Petit-Lancy, 1997), Vol 21A, p. 1101.
[2] GREENWALD, M, *et al*., Nucl. Fusion. **37,** (1997) 793.
[3] KINSEY, J.E., WALTZ, R.E. and SCHISSEL, D.P., Proc. 24th Eur. Conf on Controlled Fusion and Plasma Physics, Berchtesgaden, Germany, 1997 (European Physical Society, Petit-Lancy, 1997), Vol 21A, p. 1081.
[4] HINTON, F.L. and STAEBLER, G.M, Phys. Fluids B **5**, (1993) 1281.
[5] LEBEDEV, V.B. and DIAMOND, P.H., Phys. Plasmas **4**, (1997) 1087.
[6] WAGNER, F. and LACKNER, K., *Physics of Plasma-Wall Interactions in Controlled Fusion*, (edited by D.E. Post and R. Behrisch, published by Plenum Press, New York in cooperation with NATO Scientific Affairs Division), Series B, Physics Vol. 131, 931 (1986).
[7] ENGELHARDT, W. and FENENBERG, W., J. Nucl. Mater. **76-77**, (1978) 518.
[8] MAHDAVI, M.A., *et. al*, Nucl Fusion **42** (2002) 52.
[9] GROEBNER, R.J., *et al*, Phys. Plasmas **9**, (2002) 2134.
[10] GROEBNER, R.J., *et al*, Plasma Phys. Control Fusion **44**, (2002) A265.
[11] MAHDAVI, M.A., *et al*., 29th EPS Conference on Plasma Phys. and Contr. Fusion, Montreux, 17-21 June 2002 ECA Vol. 26B, P-2.098 (2002)
[12] MAHDAVI, M.A., *et al*, "Consistency of the Divertor and Core Plasma Densities for Burning Plasmas", to be submitted for publication.
[13] YOKOMIZO, *et al*, Plasma Physics and Contr. Nuclear Fusion Research 1982, Vol III, IAEA, Vienna (1983) 173.
[14] ROGNLIEN, T.D., *et. al*, Contrib. Plasma Phys. **34**, (1994) 362.
[15] GROEBNER, R.J. and OSBORNE, T.H., Phys. Plasmas **5**, (1998) 1800.
[16] CARLSTROM, T.N., *et al*., Rev. Sci. Instrum. **63**, (1992) 4901.
[17] WOLF, N.S., *et al*., Proc. of 15th Int. Conf. on Plasma Surface Interactions, Gifu, 2002, to be published in J. Nucl. Mater.